ELSEVIER

Journal of Fluids and Structures 21 (2005) 257–276

JOURNAL OF FLUIDS AND STRUCTURES

www.elsevier.com/locate/jfs

The aeroelastic response of a wing section with a structural freeplay nonlinearity: An experimental investigation

C.C. Marsden, S.J. Price*

Department of Mechanical Engineering, McGill University, 817 Sherbrooke Street West, Montréal, Québec, Canada H3A 2K6

Received 20 September 2004; accepted 13 May 2005
Available online 19 September 2005

Abstract

Results are presented for subsonic wind tunnel experiments performed on a two-degree-of-freedom wing section with a structural, freeplay-type nonlinearity in the pitching degree of freedom. The experiments demonstrate the effect of the freeplay on the aeroelastic response, including the presence of limit cycle flutter for specific parameter combinations. The effects of variations in both freeplay length and frequency ratio of the underlying linear system are examined for both the damped and the limit cycle response. Time histories of the damped response are used to estimate frequency and damping values, and to predict critical flutter speeds. The amplitude and frequency of the LCO response is presented for three different freeplay lengths and five frequency ratios.

1. Introduction

Nonlinearities in aeroelastic systems can arise from both structural and aerodynamic sources, and may initiate aeroelastic instabilities both above and below the flutter speed predicted by linear theory (Dowell and Tang, 2002). Typical nonlinear responses include limit cycle oscillations, LCOs, or in some cases, chaotic response. Current research focuses on a number of different aspects of the problem (Dowell et al., 2003; Lee et al., 1999). The response of a structurally nonlinear wing section in subsonic flow has been the subject of a number of investigations, including experimental/theoretical correlations for both discontinuous (Conner et al., 1997; Tang et al., 1998a, b) and continuous (O'Neil and Strganac, 1998; Sheta et al., 2002) structural nonlinearities.

Experimental investigations into the nonlinear behavior of aeroelastic systems have been reported since 1955. Woolston et al. (1955) performed experiments using a rigid two-dimensional, two-degree-of-freedom wing section with a freeplay restoring moment in the pitching degree of freedom. They reported that for free response of the nonlinear system to an initial displacement in pitch, violent flutter could occur well below the critical flutter speed of the linear system. McIntosh et al. (1981) studied the linear and nonlinear behavior of a rigid wing section with two degrees of freedom. They demonstrated the existence of both stable and unstable amplitude-sensitive limit-cycle oscillations. Yang and Zhao (1988) studied the pitching moment freeplay type of nonlinearity in low-speed wind tunnel testing of a rigid, two-dimensional wing section model and showed that the limit-cycle amplitude grows with airspeed until the linear flutter speed is reached.

*Corresponding author.
E-mail address: stuart.price@mcgill.ca (S.J. Price).

0889-9746/$ - see front matter
doi:10.1016/j.jfluidstructs.2005.05.015

Hauenstein et al. (1992) observed periodic and nonperiodic LCOs, as well as sustained chaotic motion for a rigid wing section with structural freeplay nonlinearities in both pitch and plunge degrees of freedom. Tang and Dowell (1993) reported chaotic behavior for the free and forced response of a rigid nonlinear wing section with two degrees of freedom in pitch and plunge, where the pitch restoring moment was adjustable to allow a linear, cubic or freeplay restoring moment. O'Neil and Strganac (1998) have done extensive experimental studies of the free response to an initial disturbance of a rigid, two-degree-of-freedom wing section with a continuous (cubic) structural nonlinearity in the pitch degree of freedom. They have studied the effect of initial conditions and magnitude of nonlinear stiffness on the existence, magnitude and frequency of limit-cycle oscillations. Sheta et al. (2002) used the same experimental model to investigate the relationship between LCO frequency and amplitude with freestream velocity for a constant initial displacement.

Conner et al. (1997) have studied a three-degree-of-freedom aeroelastic section with a freeplay in the control surface hinge. They showed analytically and numerically, that a "universal" curve of response amplitude as a function of airspeed may be obtained when the system response amplitudes are normalized with respect to the size of the freeplay region. This universal response shows a region of stable damped motion and four distinct regions of LCO. Trickey et al. (2002) used the same experimental model as Conner et al. (1997), with a gust-generator to provide a variety of initial disturbances, and investigated the LCO response of the wing section as a function of the flow-rate for a number of different freeplay ranges in the flap restoring moment.

The current study is an experimental investigation into the behavior of a two-dimensional, two degree-of-freedom wing section with a structural freeplay nonlinearity in pitch. Experiments are performed for six different values of ω_h/ω_α, where ω_h/ω_α is the experimentally determined, wind-off plunge/pitch frequency ratio. The system aeroelastic response to an initial disturbance is treated as either an apparently linear, damped response or as a nonlinear limit cycle oscillation. In the damped case, the relationship between freeplay length and system frequency and damping values obtained from experimental time-history data is investigated, while for limit cycle motion, the frequency and amplitude of the LCO motion are compared for three different freeplay lengths.

2. Experimental model

In the current study, wind tunnel experiments are performed on a rigid two-dimensional NACA 0012 wing section with a 57.2 cm span and a 20.3 cm chord. The elastic axis is located at 35% of the chord aft of its leading edge. The wing section is mounted vertically in a blow-down wind tunnel with a 0.61 m × 0.91 m test-section, in which the maximum flow velocity is 45 m/s in the empty test-section. The turbulence intensity outside the boundary layers is 0.5% or less. The physical properties of the wing section are listed in Table 1. The mounting system for the wing section is based on the original design by O'Neil and Strganac (1998). It enables the wing section to oscillate freely in pitch and plunge, with an adjustable restoring force and moment in the plunge and pitch degrees of freedom, respectively. Plunge motion of the wing section is provided by a traveling carriage mounted on linear bearings fixed to the top and bottom outside surfaces of the wind tunnel test-section, as shown in Fig. 1. The pitch pulleys are mounted with rotational bearings to the traveling carriage, allowing independent pitch and plunge motion of the wing section. Restoring force and moment in the plunge and pitch directions, respectively, are provided via the plunge and pitch pulleys by spring and cable attachments as shown. The mechanisms on the top and bottom of the test-section are identical.

A nonlinear mechanism, shown in Fig. 2, is introduced in the pitch degree of freedom to allow for a pitching restoring moment freeplay region with adjustable parameters. The mechanism consists of two pitch pulleys attached together by

Table 1
Wing section physical properties

Moving mass in plunge	2.38 kg
Moving mass in pitch	0.393 kg
Wing section chord	0.203 m
Wing section span	0.572 m
Distance from elastic axis to mid-chord	0.031 m
Moment of inertia (moving mass in pitch)	0.0028 m^4
Distance from mid-chord to airfoil centre of moving mass in pitch	0.032 m
K_p, effective spring constant in plunge (measured, for coupled system)	3231 N/m
K_α, effective torsional spring constant (measured, for coupled system)	35.4 m N/rad

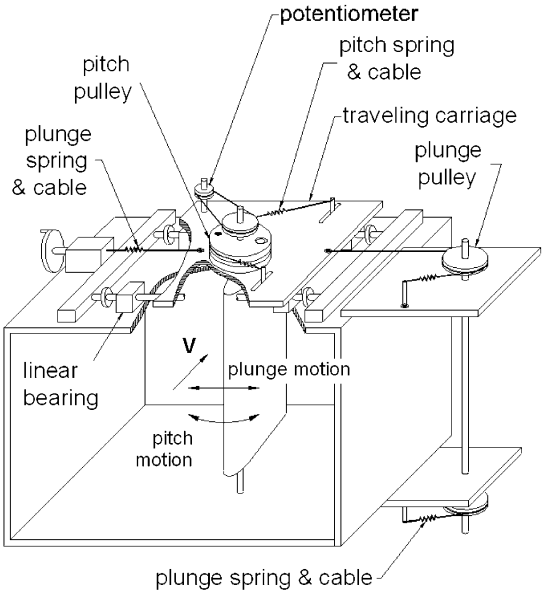

Fig. 1. Sketch of wind tunnel test-section and wing section mounting mechanism.

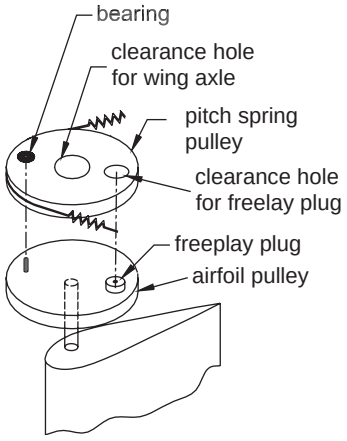

Fig. 2. Freeplay mechanism in pitch degree of freedom.

means of an off-center bearing. The bottom pulley is mounted to the wing axle and rotates with the wing. The top pulley is able to move independently of the wing axle and serves to attach the springs that provide the restoring moment. The top pulley has a circular opening that clears a circular plug fastened to the upper surface of the lower pulley. When the plug on the lower pulley is of the same size as the hole in the upper pulley, the two pulleys may not rotate independently and the moment provided by the pitch springs is transmitted directly to the wing section, resulting in a linear system. When the plug on the lower pulley is smaller than the hole in the upper pulley, the wing section may rotate through a limited range of pitch angle without any restoring moment, while there is no contact between the upper and lower pulleys. When the plug in the lower pulley contacts the edge of the hole in the upper pulley, the wing section has reached the limit of the freeplay region and the two pulleys must rotate together, causing the pitch springs to exert a restoring moment on the lower pulley and hence on the wing section. The size of the plug may be changed to vary the freeplay region length, or degrees of freeplay in pitch. The two pitch springs are mounted asymmetrically with respect to the center-line of the pitch pulley mechanism, and the degree of asymmetry may be adjusted in order to vary the restoring moment in the freeplay region (preload), as well as the location of the freeplay region within the range of pitching motion of the wing section. A typical restoring moment curve showing the freeplay region is presented in Fig. 3.

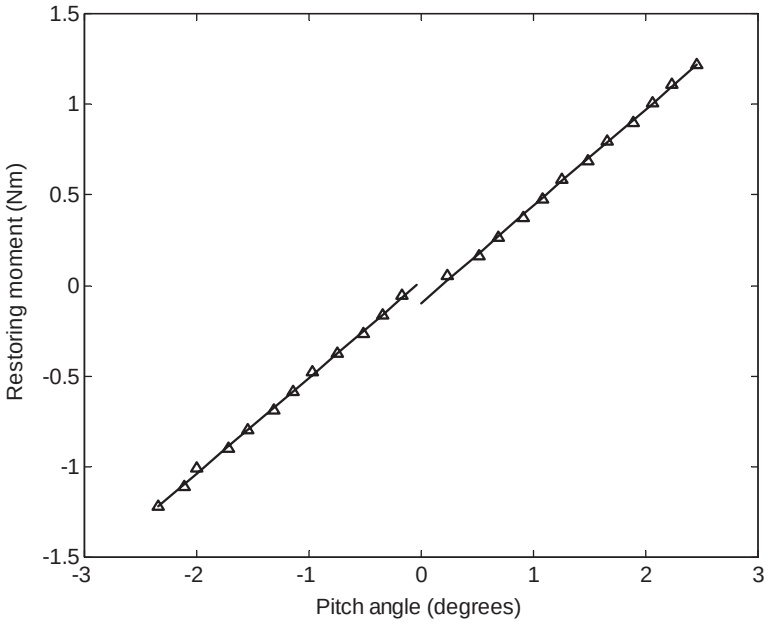

Fig. 3. Typical curve of structural restoring moment in pitch as a function of pitch angle for the nonlinear system with 0.25° freeplay: Δ, experimental data; ——, least-squares fit.

A linear variable displacement transducer (LVDT) and a potentiometer are used to record time-history records for the wing section free response to two different initial displacements in pitch and two different initial displacements in the plunge degree of freedom at each of the airspeeds tested. At each airspeed, the wing section is displaced and allowed to reach an equilibrium position in the air-flow before being released and its response recorded. Results are obtained for both decaying and limit-cycle flutter responses for the linear and three nonlinear system configurations and for a range of airspeed between zero and the linear flutter speed. The nonlinear systems correspond to freeplay lengths of 0.25°, 0.64° and 1.45° of total freeplay. For each degree of freedom, 10 000 data-points are recorded at a sampling rate of 2000 points/s. In the case of a limit cycle response, 20 000 points are recorded. The data is lowpass filtered to remove frequencies greater than 50 Hz.

3. Experimental results

For the purpose of this analysis, the time histories of the system aeroelastic response are divided into three groups by qualitative observation of the time history. The responses are classified as linearly damped as shown in Fig. 4, limit cycle flutter as shown in Fig. 5, or combined damped and limit cycle response as shown in Fig. 6.

The effect of freeplay length on the free response behavior of the aeroelastic system is examined separately for the damped response and for the sub-critical flutter or LCO response. The damped response is analyzed in a manner typical for modal testing of linear systems, in order to evaluate the impact of the freeplay length on the system frequency and damping values. Mixed damped/LCO responses were obtained for some initial conditions at almost all airspeeds up to the maximum testing speed, allowing both 'linear' and nonlinear types of aeroelastic analysis of the system. This mixed damped/LCO type of response occurred at airspeeds where limit-cycle flutter exists, and is probably a result of dry friction in the system, damping out a purely LCO type of response. Purely limit-cycle responses are analyzed for LCO frequency and amplitude.

3.1. Linear system analysis

The results for the linear system frequency and damping trends with airspeed are shown in Figs. 7–9 for the six frequency ratios tested. Frequency values are calculated from the time histories using the maximum, zero crossing, and

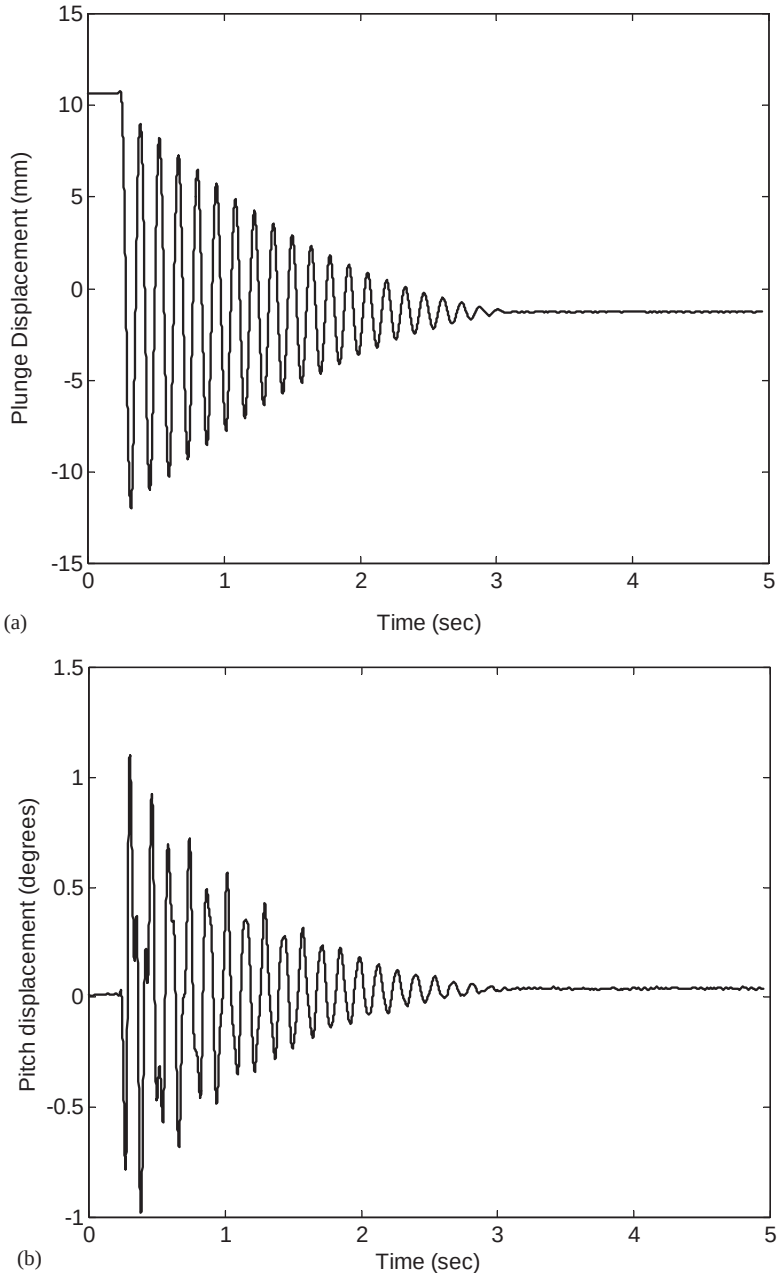

Fig. 4. Typical 'linear-type' damped response for the linear system at $V = 5.67\,\mathrm{m/s}$ and $\omega_h/\omega_\alpha = 0.398$: (a) Plunge response to an initial displacement in plunge; (b) pitch response induced by plunge displacement.

minimum displacement values and their respective time coordinates. Average values are taken over 3 to 4 cycles of motion and for two different initial displacements in pitch and four initial displacements in plunge. Damping values were calculated using the logarithmic decrement method and averaged over 3 to 4 cycles for positive and negative initial displacements in both degrees of freedom. For a typical case ($\omega_h/\omega_\alpha = 0.398$) the standard deviation for the mean frequency range from 0.042 to 0.082 and for damping from 0.011 to 0.018.

Fig. 7 shows a typical aeroelastic frequency coalescence with airspeed for six different frequency ratios. The pitch frequency is the same in all six cases ($\omega_\alpha = 18.0\,\mathrm{Hz}$), with the structural stiffness in plunge being varied and effectively giving the frequency ratio. Figs. 8 and 9 show the viscous damping trends in the pitch and plunge degrees of freedom,

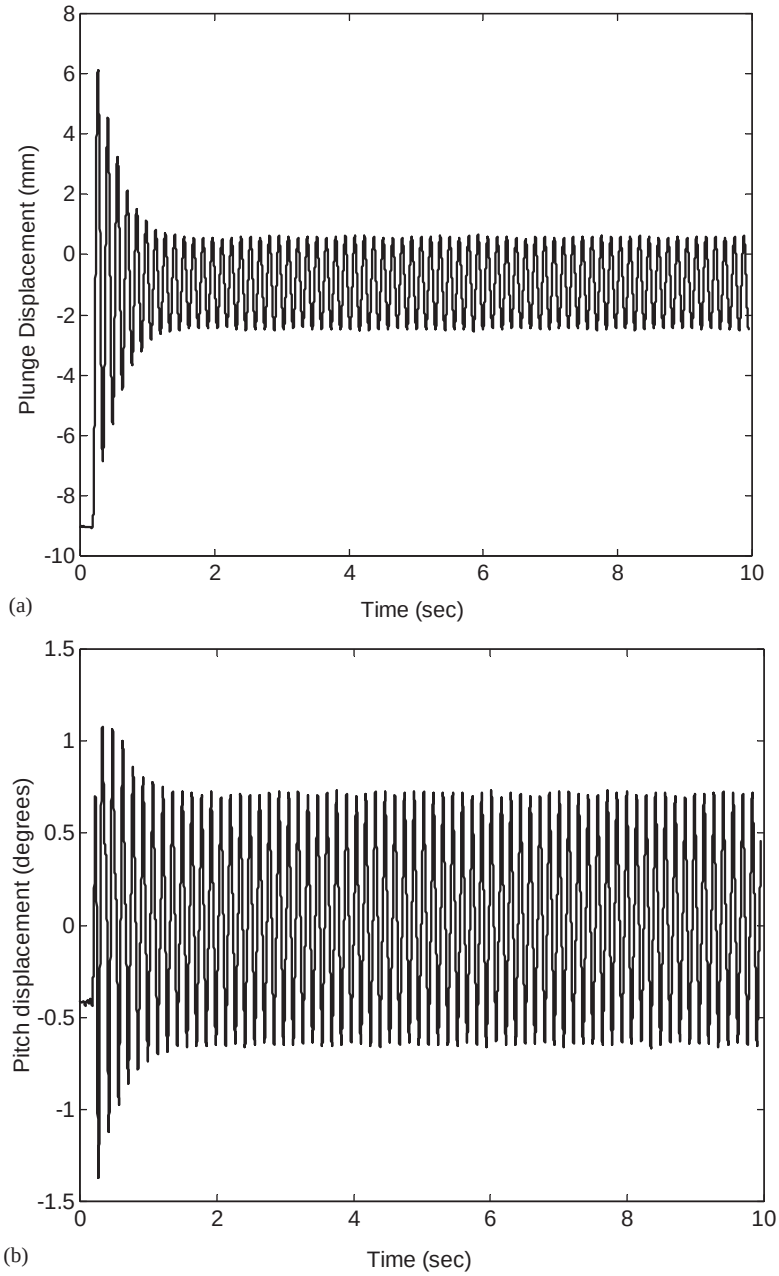

Fig. 5. Typical limit cycle response for the nonlinear system with a freeplay length of 0.64° at $V = 23.4\,\mathrm{m/s}$ and $\omega_h/\omega_\alpha = 0.366$: (a) Plunge response to an initial displacement in plunge; (b) pitch response induced by plunge displacement.

respectively. In all the cases, the damping initially increases with airspeed and achieves a maximum at an airspeed that appears to depend on the system frequency ratio, with the maximum damping value decreasing with increasing frequency ratio. The damping then decreases with increasing airspeed with a steeper slope than at the lower airspeeds, and approaches zero damping at an airspeed that again varies with the system frequency ratio. The shape of the curves in the pitch and plunge degrees of freedom are different. The pitch curve is steeper and more symmetrical about the position of maximum damping. It also has a more pronounced peak at the maximum damping value, which occurs at a lower airspeed than is the case in the plunge degree of freedom. The plunge damping peaks at a higher airspeed than the

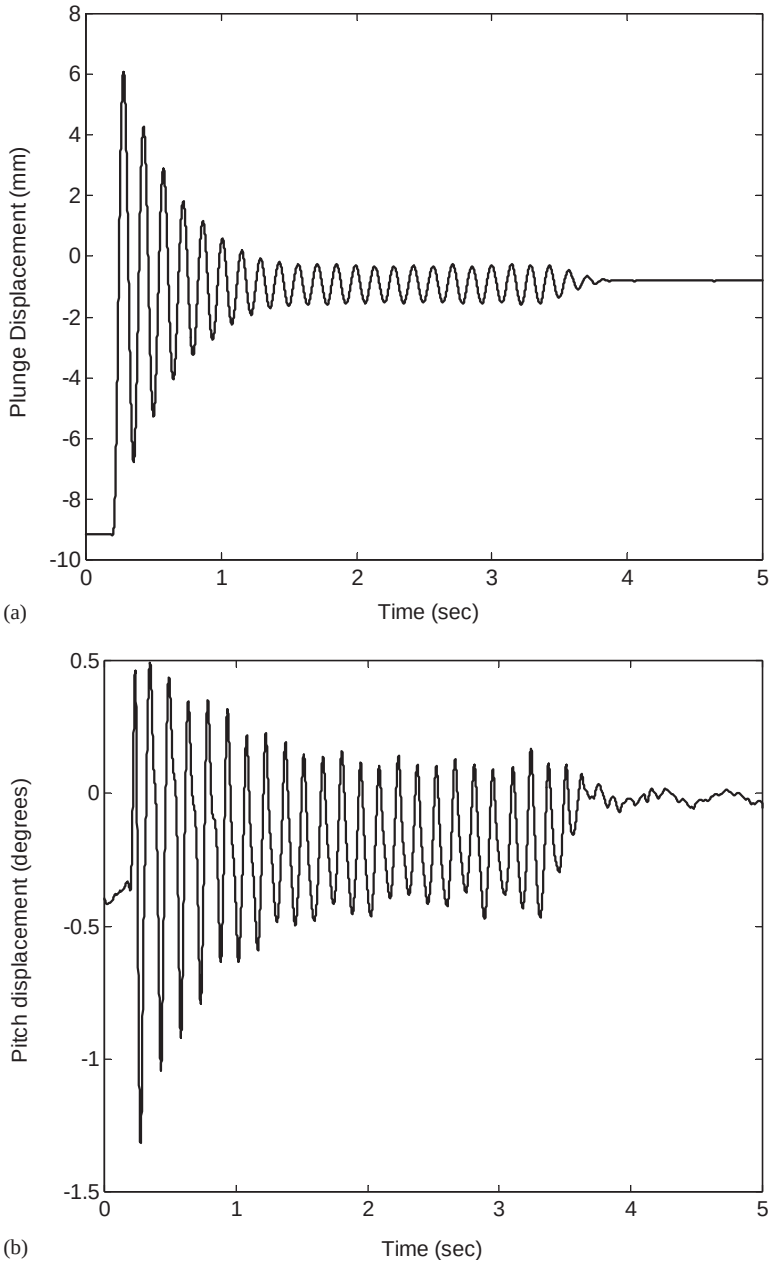

Fig. 6. Typical mixed damped and limit cycle response for the nonlinear system with a freeplay length of 0.25° at $V = 23.4\,\mathrm{m/s}$ and $\omega_h/\omega_\alpha = 0.366$: (a) Plunge response to an initial displacement in plunge; (b) pitch response induced by plunge displacement.

pitch damping, and in some cases does not peak at all within the range of airspeeds tested. The final decrease in damping towards zero is more abrupt in this degree of freedom.

In order to avoid damaging the model and structural restoring force mechanism, the system was never run to the critical flutter speed. For this reason, it was necessary to predict the critical flutter speed from the sub-critical data available. Numerical simulations for an aeroelastic system using unsteady aerodynamics combined with structural parameters similar to the experimental values were used to estimate the critical flutter speeds for the six experimental frequency ratios, and the results are listed in Table 2. These results are difficult to validate without actual test data at the divergent flutter speed, or an accurate numerical model. However, in Fig. 10, the damping curves in the pitch degree of

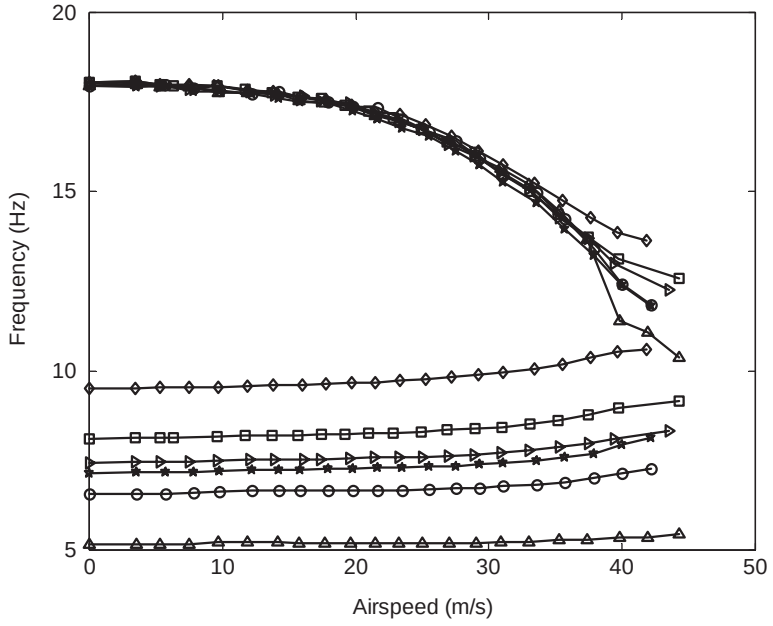

Fig. 7. Pitch and plunge frequencies for the linear system as a function of airspeed: Δ, $\omega_h/\omega_\alpha = 0.287$; ○, $\omega_h/\omega_\alpha = 0.366$; ★, $\omega_h/\omega_\alpha = 0.398$; ▷, $\omega_h/\omega_\alpha = 0.413$; □, $\omega_h/\omega_\alpha = 0.449$; ◇, $\omega_h/\omega_\alpha = 0.526$.

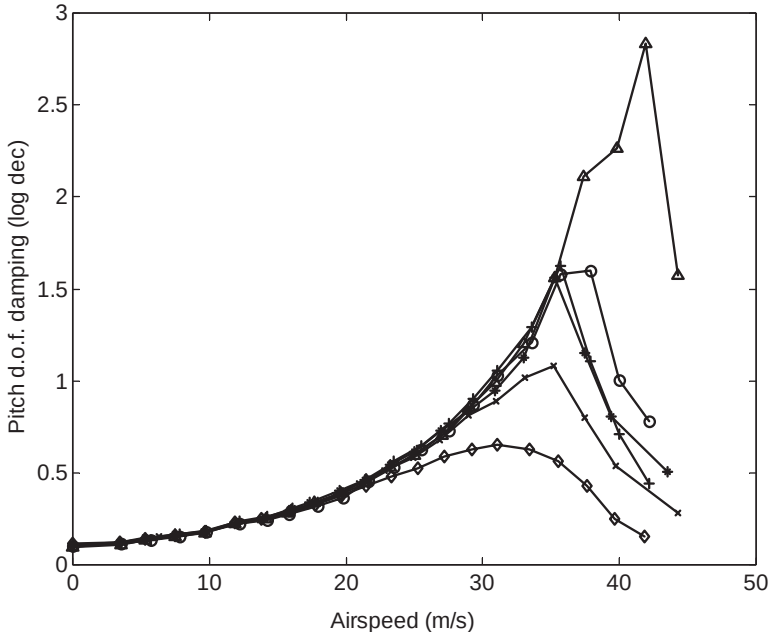

Fig. 8. Damping logarithmic decrement in pitch as a function of airspeed for linear system: Δ, $\omega_h/\omega_\alpha = 0.287$; ○, $\omega_h/\omega_\alpha = 0.366$; +, $\omega_h/\omega_\alpha = 0.398$; *, $\omega_h/\omega_\alpha = 0.413$; x, $\omega_h/\omega_\alpha = 0.449$; ◇, $\omega_h/\omega_\alpha = 0.526$.

freedom are shown as a function of V/V^*, where the airspeed has been normalized with respect to the predicted flutter speed, V^*. Compared to Fig. 8, it can be seen that an extrapolation of the damping trends indicates that zero damping will occur at approximately $V/V^* = 1$ for all frequency ratios, indicating that the estimated flutter speeds may be considered reasonable approximations.

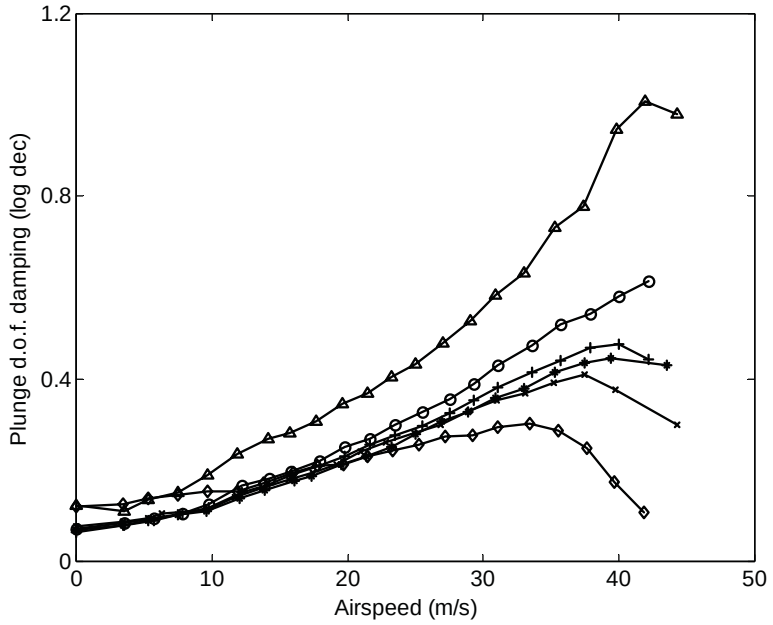

Fig. 9. Damping logarithmic decrement in plunge as a function of airspeed for linear system: Δ, $\omega_h/\omega_\alpha = 0.287$; ○, $\omega_h/\omega_\alpha = 0.366$; +, $\omega_h/\omega_\alpha = 0.398$; *, $\omega_h/\omega_\alpha = 0.413$; x, $\omega_h/\omega_\alpha = 0.449$; ◇, $\omega_h/\omega_\alpha = 0.526$.

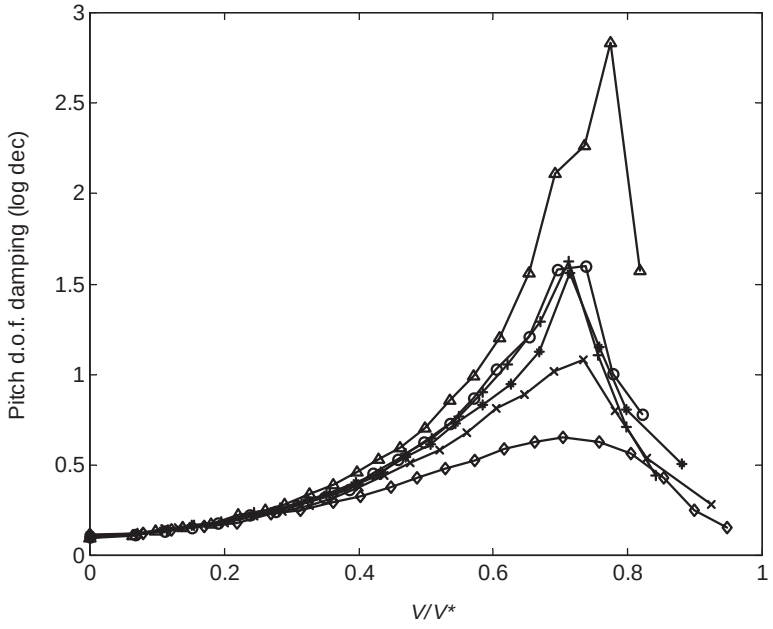

Fig. 10. Damping logarithmic decrement in pitch as a function of normalized airspeed for linear system: Δ, $\omega_h/\omega_\alpha = 0.287$; ○, $\omega_h/\omega_\alpha = 0.366$; +, $\omega_h/\omega_\alpha = 0.398$; *, $\omega_h/\omega_\alpha = 0.413$; x, $\omega_h/\omega_\alpha = 0.449$; ◇, $\omega_h/\omega_\alpha = 0.526$.

The use of the "flutter margin" (Zimmerman and Weissenburger, 1964) is an alternative to relying on the modal damping trend to predict the onset of flutter. The flutter margin is a quantity that is calculated from the experimentally obtained values of frequency and damping. It decreases in an approximately quadratic manner with increasing dynamic pressure until it reaches zero at the flutter speed. The advantage of using the flutter margin over the modal damping lies

Table 2
Estimated linear flutter speeds

Frequency ratio, ω_h/ω_α	0.287	0.366	0.398	0.413	0.449	0.526
Flutter speed from numerical simulation (m/s)	54.1	51.4	50.1	49.4	47.9	44.1
Flutter speed from flutter margin (m/s)	50.5	49.8	48.3	47.2	45.5	44.8

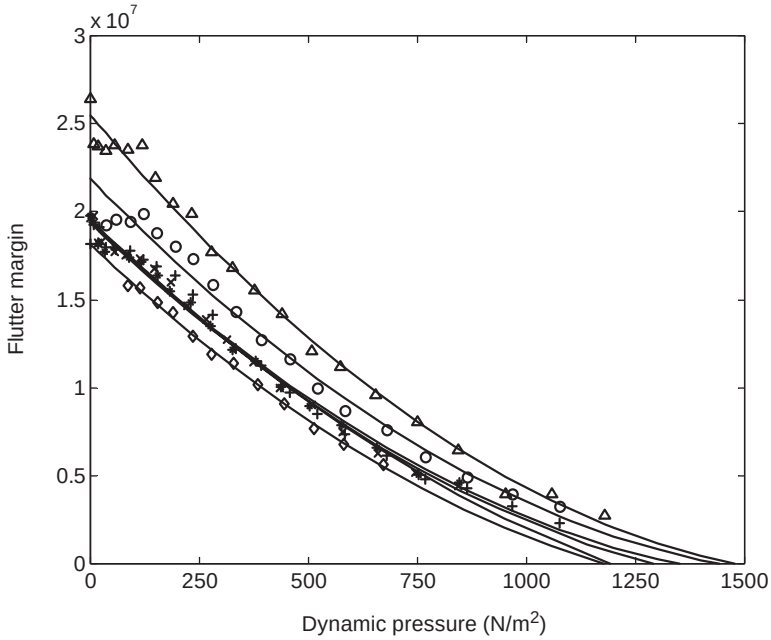

Fig. 11. Flutter margin as a function of dynamic pressure for linear system: Δ, $\omega_h/\omega_\alpha = 0.287$; ○, $\omega_h/\omega_\alpha = 0.366$; +, $\omega_h/\omega_\alpha = 0.398$; *, $\omega_h/\omega_\alpha = 0.413$; x, $\omega_h/\omega_\alpha = 0.449$; ◇, $\omega_h/\omega_\alpha = 0.526$.

in its smooth variation with airspeed, making it possible to predict the onset of flutter from data obtained at airspeeds as low as 50% of the flutter speed.

Fig. 11 shows the variation of flutter margin with dynamic pressure for the linear systems tested, and the predicted flutter speeds obtained by extrapolating from the data-points shown are listed in Table 2. The linear flutter speeds obtained using the flutter margin are within 6% of the values obtained earlier from the numerical simulation. This gives a high degree of confidence in both the numerical simulation and the flutter-margin method.

The series of experiments done on the linear system provides a baseline against which frequency and damping trends for the nonlinear system can be compared. They also provide estimates of the critical divergent flutter speeds and wind-off frequency ratios for each of the aeroelastic systems tested.

3.2. Nonlinear system response

3.2.1. Damped response

The nonlinear aeroelastic system does not always respond to an initial displacement in a manner that is obviously "nonlinear". In many cases, and in particular for airspeeds well below the critical flutter speed, the response is qualitatively linear. For this reason, it is of interest to examine the trends in the modal parameters obtained from typical modal testing and to compare the results obtained from the linear and nonlinear systems. Figs. 12 and 13 compare the damping trends with airspeed in pitch and plunge, respectively, for one particular frequency ratio. Values obtained for the linear case are compared to results for the three nonlinear systems. For a nonlinear system, damping values will vary depending on the number of cycles used in the calculation. In order to produce consistent results, damping values for

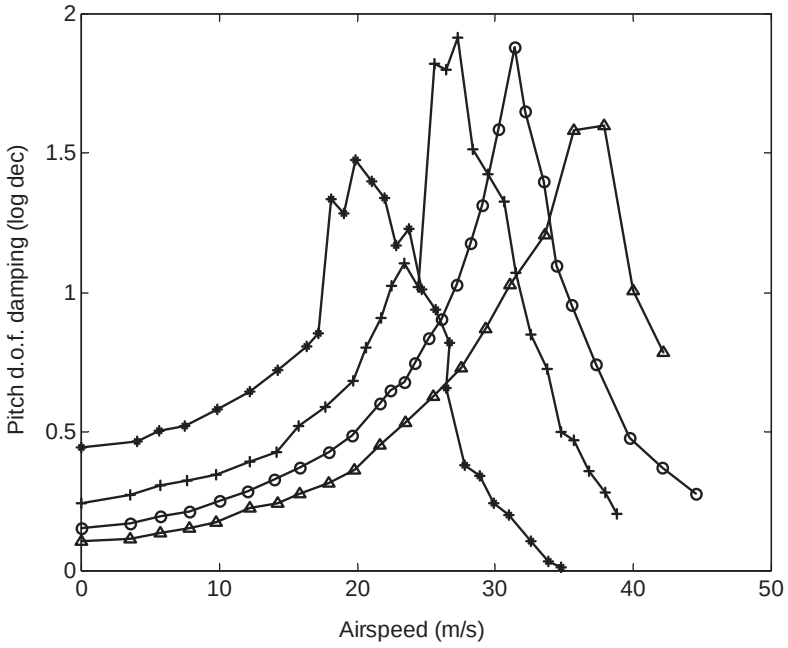

Fig. 12. Damping logarithmic decrement in pitch as a function of airspeed for $\omega_h/\omega_\alpha = 0.366$: Δ, linear system; ○, 0.25° freeplay; +, 0.64° freeplay; *, 1.45° freeplay.

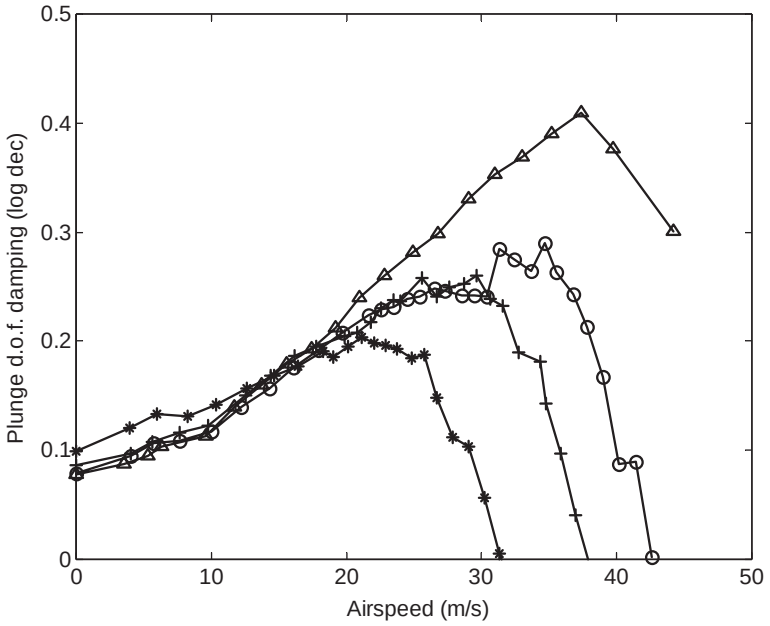

Fig. 13. Damping logarithmic decrement in plunge as a function of airspeed for $\omega_h/\omega_\alpha = 0.449$: Δ, linear system; ○, 0.25° freeplay; +, 0.64° freeplay; *, 1.45° freeplay.

the nonlinear cases are calculated using the same magnitude of displacement and the same number of peaks and valleys as was the case for the linear system (3–4 cycles), and averaging values obtained for positive and negative initial displacements.

The shape of the pitch-degree-of-freedom damping curve is similar in all four cases shown in Fig. 12, with the maximum value of damping being followed by a rapid decrease toward zero as the airspeed approaches the flutter speed. The introduction of the freeplay nonlinearity increases the system damping at zero airspeed and has the effect of shifting the peak in the curve to a lower airspeed. The increase in damping at lower airspeeds may be attributed to the system viscous damping, because the viscous damping is proportional to the velocity. The freeplay region in this series of experiments is approximately centered on the zero pitch displacement position, and when the wing section is oscillating, the maximum velocity in pitch is attained at zero displacement. As a result, within the freeplay region the restoring moment is essentially zero while the viscous damping forces are at a maximum, and the system damping increases.

The damping increases with freeplay size for lower airspeeds, and decreases with freeplay size as the airspeed approaches the linear flutter speed. The curves also approach zero damping values at lower airspeeds for increasing freeplay size, even though the linear flutter speed is the same for all the cases. Fig. 13 shows similar results for the plunge degree of freedom. In this case, the damping values at low airspeeds are similar regardless of freeplay size, and at higher airspeeds, the apparent damping increases significantly with airspeed. The maximum damping peak for the plunge degree of freedom is shifted to a lower airspeed for the nonlinear systems, as was the case for the pitch degree of freedom. It is evident from the curves shown in Figs. 12 and 13 that the damping values are a function of the freeplay gap size, and if both axes are scaled, they will lie on the same approximate curve, although the scaling factors are not a simple function of freeplay length.

The frequency trends with airspeed for pitch and plunge are shown in Fig. 14 for one of the six frequency ratios. The shapes of the linear and nonlinear curves are similar, although the values obtained for the largest freeplay size are erratic. As was the case with the damping curves, it is evident that the frequency curve is a function of the freeplay gap size. As the gap size increases, the pitch frequency decreases at all airspeeds, while the plunge frequency stays the same at low airspeeds, and increases slightly with increasing freeplay length at higher airspeeds. If the curves are extrapolated to predict frequency coalescence as an indicator of the critical flutter speed, the predicted flutter speed decreases with increasing freeplay length.

3.2.2. *Flutter speed analysis*

The results presented in the previous section show that when a freeplay nonlinearity is introduced in the pitch degree of freedom, the flutter speed estimated by extrapolation of the damping curve decreases with increasing freeplay size. When the flutter margin method is used to estimate the flutter speeds for the linear and nonlinear systems, the results for all the frequency ratios are similar to those shown in Fig. 15 for $\omega_h/\omega_\alpha = 0.413$. In Fig. 15, a quadratic curve is fitted to the data-points obtained using the flutter margin method described earlier. For the linear case and the smallest of the freeplay sizes, the data represent tests done between 0 and 37 m/s. For the 0.64° and 1.45° freeplay cases, the airspeed ranges used to curve fit are from 0 to 30 and 0–27 m/s, respectively. The decrease in the number of data-points used to curve fit with increasing freeplay size is a result of the increasing amplitude of LCOs for the larger gap sizes at higher airspeeds, which make it impossible to obtain reasonable damping values. The effect of the size of the freeplay region is evident, and is the same as for the modal damping, with the estimated flutter speeds decreasing significantly with increasing freeplay length. Predicted flutter speeds from Fig. 15 are listed in Table 3.

3.2.3. *Limit-cycle oscillations*

For the nonlinear systems, all but one of the frequency ratios tested exhibited limit-cycle flutter at airspeeds below the critical flutter speed for the equivalent linear system. Limit-cycle oscillations with amplitudes as large as 40 times the freeplay gap size were observed. The length of the freeplay region in the pitch degree of freedom has an effect on the presence of limit cycle oscillations in the system response as well as on the amplitude and frequency of the resulting limit cycle motion. The range of airspeeds for which LCOs occur depends on both the system wind-off frequency ratio and the freeplay length.

3.2.3.1. Existence of LCO. For the case of the smallest frequency ratio, $\omega_h/\omega_\alpha = 0.287$, the response to initial displacements in either pitch or plunge was always damped, and no LCO motion was observed. When the plunge stiffness was increased to obtain a frequency ratio of $\omega_h/\omega_\alpha = 0.366$, two regions of LCO motion were observed. The first region extends from 20 to 27 m/s and is characterized almost exclusively by damped LCO motion. In this damped LCO motion, as exemplified by Fig. 6, an apparent LCO is obtained which then damps out after the existence of a certain number of cycles. The damping of the LCO motion is most likely a result of the dry friction in the system. The number of cycles existing in this LCO motion before it damps out are shown as a function of airspeed and initial displacement in plunge in Fig. 16. In general, the number of limit cycles in the response before the motion damps to zero

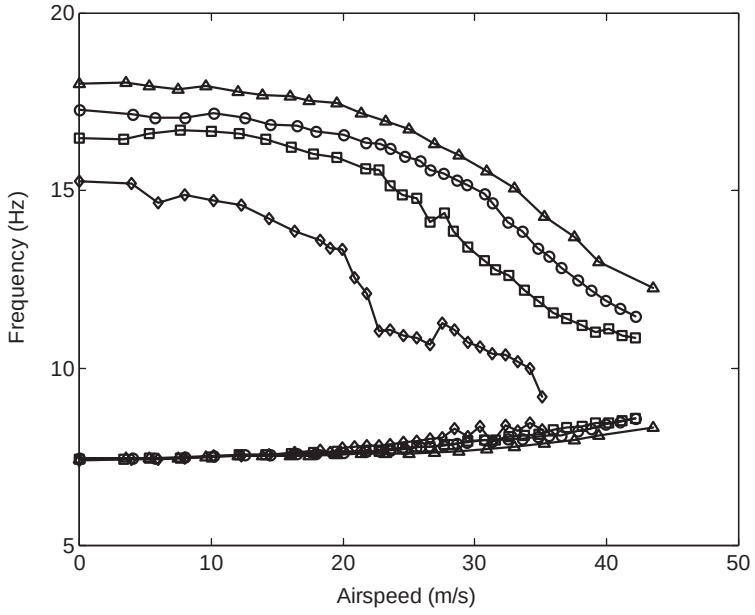

Fig. 14. Pitch and plunge frequencies as a function of airspeed for $\omega_h/\omega_\alpha = 0.413$: Δ, linear system; ○, 0.25° freeplay; □, 0.64° freeplay; ◇, 1.45° freeplay.

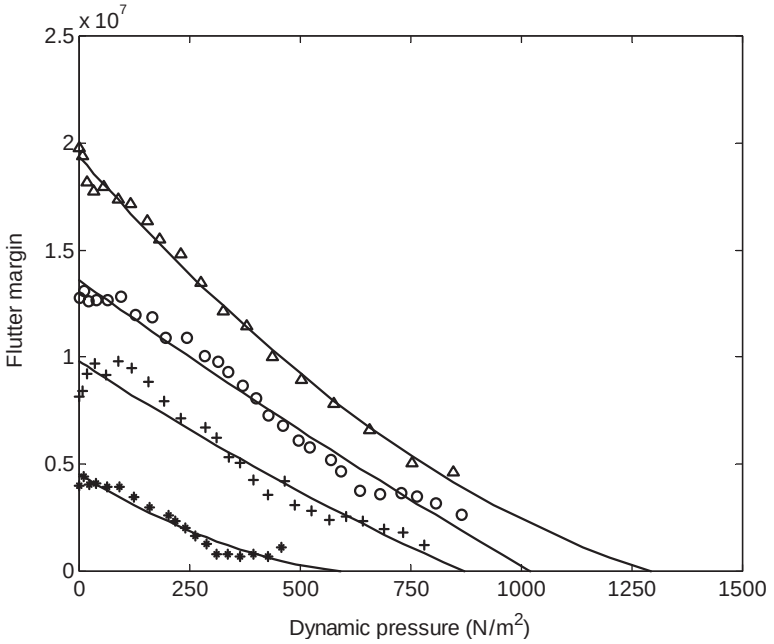

Fig. 15. Flutter margin as a function of dynamic pressure for $\omega_h/\omega_\alpha = 0.413$: Δ, linear system; ○, 0.25° freeplay; +, 0.64° freeplay; *, 1.45° freeplay.

Table 3
Flutter speeds for linear and nonlinear system at $\omega_h/\omega_\alpha = 0.413$ (estimated using flutter margin)

Freeplay gap size (deg)	0.0	0.25	0.64	1.45
Flutter speed (m/s)	47.2	41.8	38.7	31.6

varies with airspeed and initial displacement, but is repeatable within two or three cycles if the experiment is repeated at the same airspeed and initial displacement. The number of LCO cycles before the motion damps out increases with increasing positive initial displacements in plunge and decreases with increasingly negative displacements. This reflects the relationship between initial displacement and the energy stored in the plunge springs. Because the wing section has a

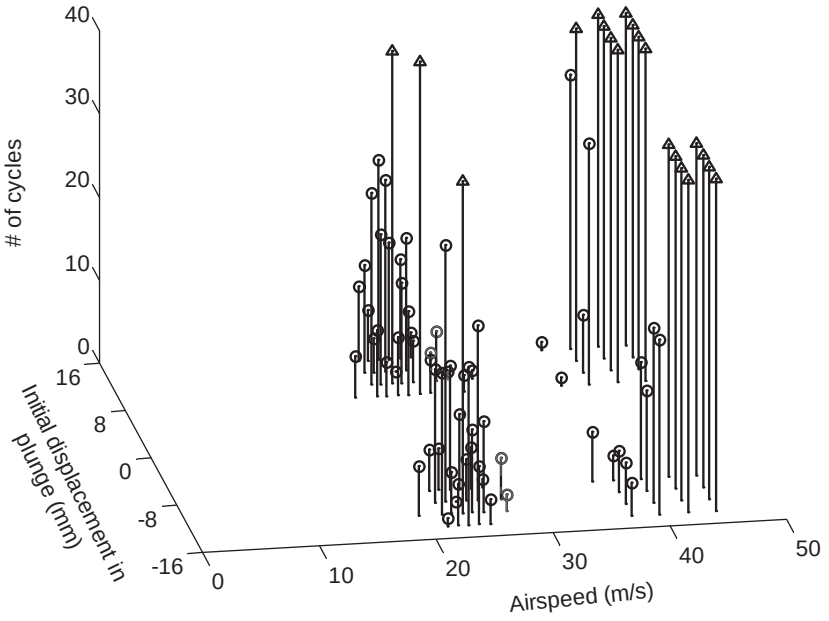

Fig. 16. Occurrence of LCOs as a function of airspeed and initial displacement in plunge for $\omega_h/\omega_\alpha = 0.413$ and 0.25° of freeplay in pitch: ○, number of cycles of damped LCO motion; Δ, region of full undamped LCO motion.

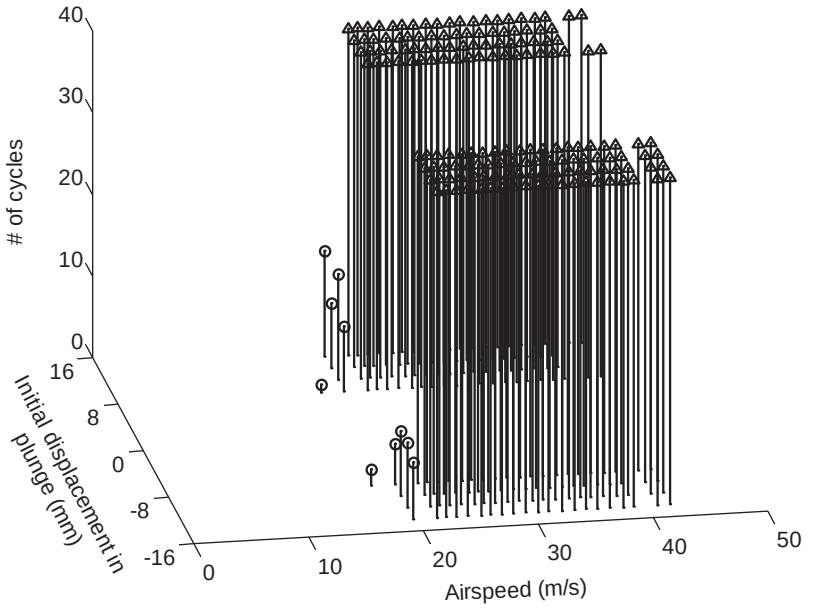

Fig. 17. Occurrence of LCOs as a function of airspeed and initial displacement in plunge for $\omega_h/\omega_\alpha = 0.413$ and 0.64° of freeplay in pitch: ○, number of cycles of damped LCO motion; Δ, region of full undamped LCO motion.

slightly non zero initial angle of attack, the equilibrium pitch angle increases with increasing airspeed. Thus, the lift created at each airspeed moves the wing section away from zero displacement and consequently, the same positive and negative initial displacements are asymmetric about the equilibrium plunge position.

Between 27 and 36 m/s, the system response returns to a fully damped type of response similar to that shown in Fig. 4. At 36 m/s, the damped type of limit cycle response returns, and with increasing airspeed the response rapidly becomes a fully developed LCO at all airspeeds until the maximum airspeed tested. As the freeplay length is increased, the two regions of freeplay shown in Fig. 16 approach each other, and the LCO motion becomes more robust, with fewer regions of damped-out LCO. Fig. 17 is similar to Fig. 16, but for 0.64° of freeplay. The limit-cycle response begins at

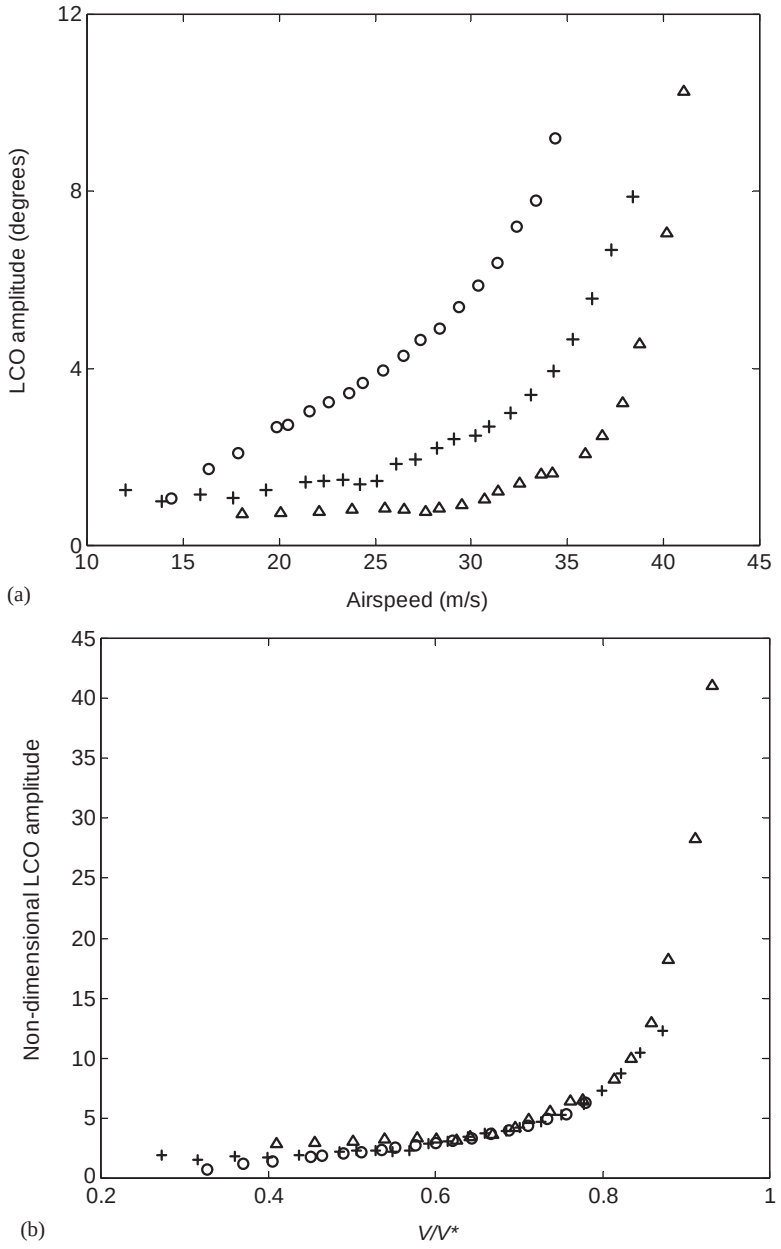

Fig. 18. LCO amplitude in pitch as a function of airspeed for $\omega_h/\omega_\alpha = 0.526$: Δ, 0.25° freeplay; +, 0.64° freeplay; ○, 1.45° freeplay: (a) LCO amplitude in degrees and airspeed in m/s; (b) LCO amplitude normalized with respect to freeplay length and airspeed normalized with respect to the linear flutter speed.

20 m/s, the same airspeed as for the case with 0.25° of freeplay. The LCO motion for 0.64° of freeplay is rarely damped and continues without interruption until the maximum test speed is reached. When the freeplay length is increased to 1.45°, the LCO distribution is similar to that for the 0.64° case, except that the LCO motion appears at a lower airspeed (16 m/s). Results for the other frequency ratios tested are not shown here, but are similar, with the exception that the two distinct ranges of airspeed for LCO motion disappear with increasing frequency ratio.

3.2.3.2. LCO amplitude. The amplitude of the LCO motion is a function of the freeplay length, while the frequency appears to be independent of the freeplay. Fig. 18(a) compares the LCO amplitudes in the plunge degree of freedom for

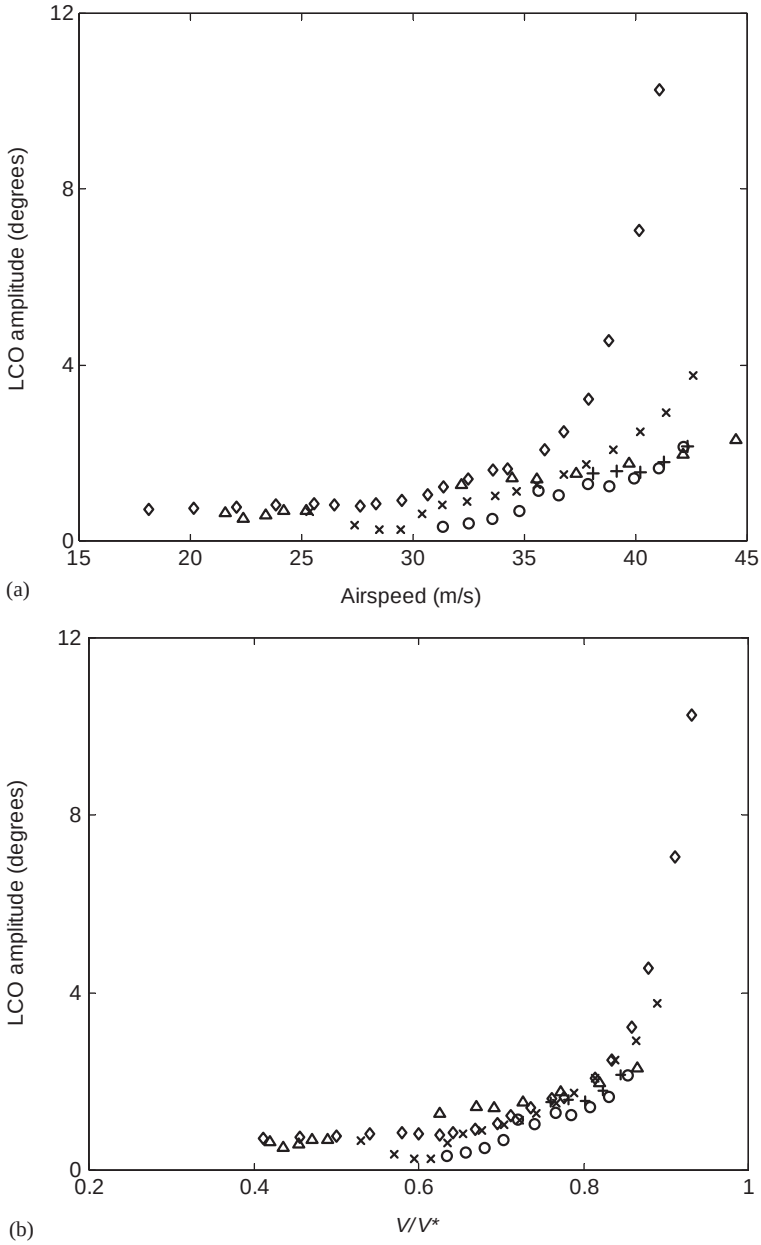

Fig. 19. LCO amplitude in pitch as a function of airspeed for a freeplay length of 0.25°: Δ, $\omega_h/\omega_\alpha = 0.366$; +, $\omega_h/\omega_\alpha = 0.398$; ○, $\omega_h/\omega_\alpha = 0.413$; x, $\omega_h/\omega_\alpha = 0.449$; ◇, $\omega_h/\omega_\alpha = 0.526$: (a) LCO amplitude in degrees and airspeed in m/s; (b) LCO amplitude in degrees and airspeed normalized with respect to the linear flutter speed.

the three freeplay lengths, for $\omega_h/\omega_\alpha = 0.526$. The LCO amplitudes shown are obtained from the filtered data by averaging the difference in magnitude between the peaks and valleys of the pitch and plunge displacement curves over 30 cycles. A typical standard deviation for this result is 0.006–0.007 in pitch and 0.001–0.003 in plunge. In Fig. 18(b), the same information is presented, but the LCO amplitudes are normalized with respect to the freeplay length, and the airspeed is normalized with respect to the linear flutter speed. LCO amplitudes in plunge behave in a similar way, and are not shown here. Results obtained for the other frequency ratios tested are consistent. When the data is normalized with respect to the freeplay length and the linear flutter speed, the amplitudes of the LCO motion at any given frequency ratio all lie on the same curve. The amplitudes increase relatively slowly and almost linearly at airspeeds below 60% of the linear flutter speed, and then the curve starts to rise more rapidly. Between 80% and 100% of the linear flutter speed, the increase in LCO amplitude with increasing airspeed is quite dramatic, apparently approaching extremely large amplitudes at the critical linear flutter speed.

Fig. 19(a) compares LCO amplitudes for the five frequency ratios at the smallest freeplay length, 0.25°. Although the gap size is the same, the variations of LCO amplitude with airspeed are very different. In Fig. 19(b) the data is normalized with respect the critical airspeed, V^*. In this case, although the scaling factors bring the four curves closer together, they do not obviously fall on the same line. As the airspeed approaches critical flutter, the LCO amplitudes are larger for the larger frequency ratios. This may be a result of error in the predicted flutter speeds. However, bearing in mind the successful normalization shown in Fig. 18(b), it suggests that the LCO amplitude depends on both the frequency ratio of the underlying linear system and the freeplay length.

3.2.3.3. LCO frequency. The frequency of the LCO is not a function of the freeplay length. Fig. 20 compares the LCO frequencies for the three freeplay lengths, at $\omega_h/\omega_\alpha = 0.413$. The frequency increases with increasing airspeed, but all three freeplay lengths yield the same frequency of LCO motion for any given airspeed.

Fig. 21(a) compares the LCO frequencies observed at the five different frequency ratios, for a freeplay length of 0.25°, and it is clear that the LCO frequency depends very strongly on the frequency ratio of the underlying linear system. In Fig. 21(b), the frequencies shown in Fig. 21(a) are normalized with respect to the wind-off plunge frequencies, and the result suggests that the LCO frequency is a simple function of the underlying linear system frequencies. The relatively small spread seen between the different curves in Fig. 21(b) may be because the data were normalized with respect to the wind-off measured experimental frequencies instead of the uncoupled natural frequencies of the system.

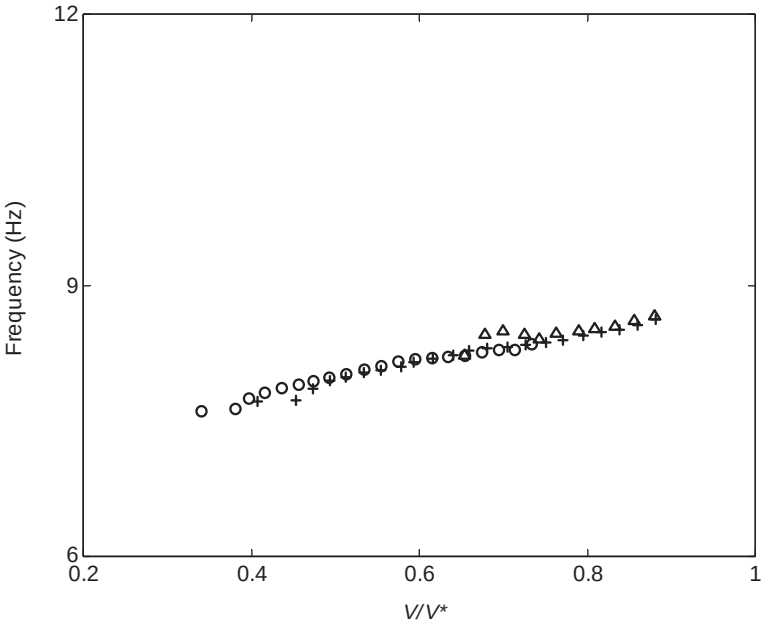

Fig. 20. LCO frequency as a function of nondimensional airspeed for $\omega_h/\omega_\alpha = 0.413$: Δ, 0.25° freeplay; +, 0.64° freeplay; ○, 1.45° freeplay.

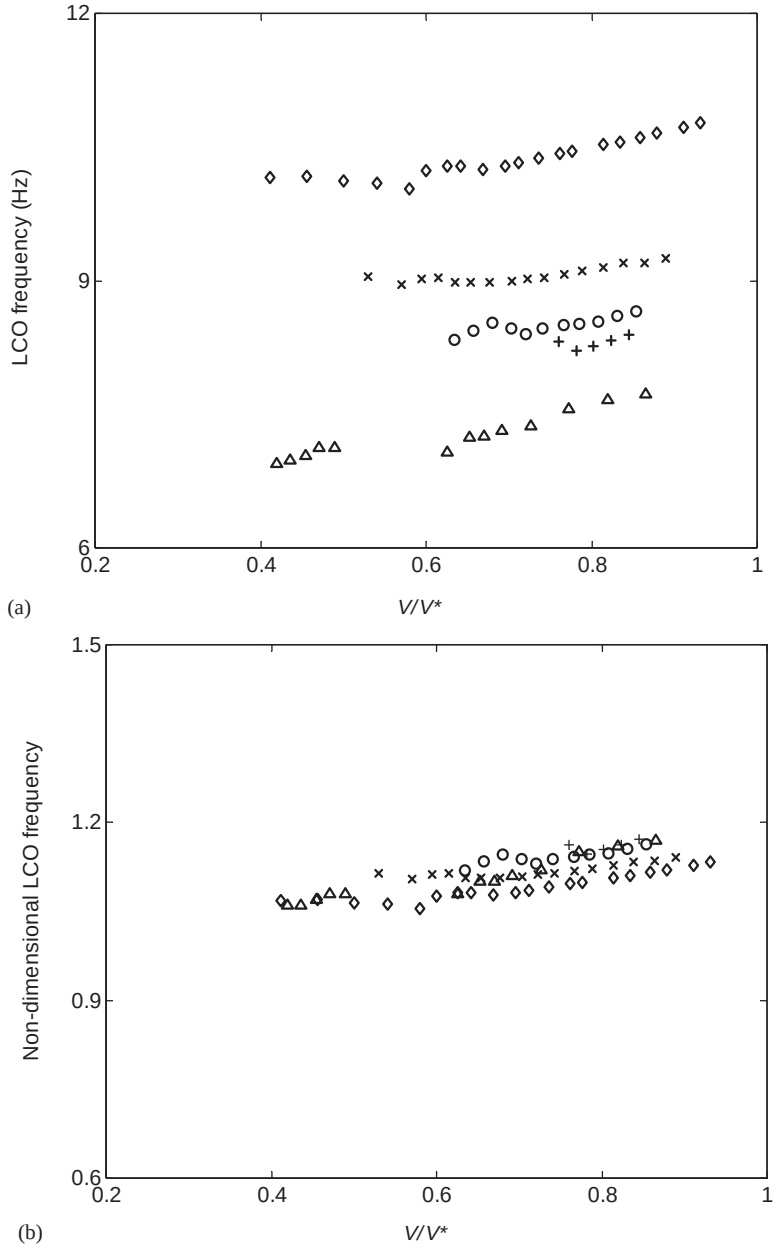

Fig. 21. LCO frequency as a function of normalized airspeed for freeplay length of 0.25°: Δ, $\omega_h/\omega_\alpha = 0.366$; +, $\omega_h/\omega_\alpha = 0.398$; ○, $\omega_h/\omega_\alpha = 0.413$; x, $\omega_h/\omega_\alpha = 0.449$; ◇, $\omega_h/\omega_\alpha = 0.526$: (a) LCO frequency in Hz; (b) LCO frequency normalized with respect to the wind-off plunge frequencies.

4. Conclusions

Three types of behavior are identified for the aeroelastic response of a structurally nonlinear wing section to an initial displacement in one of its two degrees of freedom: a damped response typical of linear systems; a sub-critical flutter characterized by limit-cycle oscillations; and a response containing both damped and limit-cycle oscillations, but where the LCO motion is unstable and eventually damps to zero.

For the damped response of the nonlinear system, values of frequency and damping vary with airspeed in a manner similar to that obtained for a linear system. It is shown that these parameters scale as a function of the freeplay gap size,

with the damping curve being shifted to lower airspeeds with increasing gap size, while the frequency in pitch decreases with increasing gap size. Flutter speeds predicted from modal damping trends are affected by the size of the freeplay, with the flutter speed decreasing with increasing freeplay length. Similar results are also obtained when the flutter speed is estimated using the flutter margin method, with the predicted flutter speeds again decreasing with increasing freeplay length.

For the nonlinear system, sub-critical flutter or limit-cycle oscillations occur at airspeeds well below the flutter speed for the equivalent linear system, with amplitudes of up to 40 times the freeplay length observed for the smallest freeplay size tested. The amplitude of the LCO increases with increasing airspeed, with the slope of the curve becoming almost vertical as the airspeed approaches critical flutter. It is shown that the amplitudes of the LCO motion scales as a function of the freeplay length and the frequency ratio of the underlying linear system. This result is in agreement with the results presented by Tang and Dowell (1993) and by Conner et al. (1997). Conner et al. (1997) have studied the behavior of a three-degree-of-freedom airfoil section with a control surface and a nonlinear restoring force in the control surface degree of freedom. They show that for the limit cycle oscillations of an airfoil section with control surface freeplay, the nonlinear LCO response is a function of the freeplay gap size. In the present study, however, the frequency of the LCO appears to be independent of the gap size. This may be because the freeplay sizes in the present study are much smaller with respect to the LCO amplitudes than in the experiments performed by Conner et al., with the result that the present study does not reveal the relationship between gap size and LCO frequency. The frequency of the LCO motion is, however, shown to scale with the frequency ratio of the underlying linear system.

The presence of limit-cycle oscillations depends on the freeplay length, with only damped LCOs being present at some airspeeds. The term "damped LCO" is used to describe a transient response that appears to become a stable LCO, but after several cycles of oscillation, damps quite suddenly (within one oscillation) to zero. This type of behavior was observed for all of the frequency ratios tested, and appears to be a result of the nonlinear damping. The friction damping in the experimental apparatus, particularly in the plunge degree of freedom is not negligible, and is probably responsible for the damped LCO behavior.

Acknowledgements

The authors would like to acknowledge the support they received from the Natural Sciences and Engineering Research Council of Canada (NSERC). The authors also wish to thank Dr B.H.K. Lee and the NRC Institute for Aerospace Research for the loan of the test-section and experimental apparatus.

References

Conner, M.D., Tang, D.M., Dowell, E.H., Virgin, L.N., 1997. Nonlinear behaviour of a typical airfoil section with a control surface freeplay: a numerical and experimental study. Journal of Fluids and Structures 11, 89–109.

Dowell, E., Tang, D., 2002. Nonlinear aeroelasticity and unsteady aerodynamics. AIAA Journal 40, 1697–1707.

Dowell, E., Edwards, J., Strganac, T., 2003. Nonlinear aeroelasticity. Journal of Aircraft 40, 857–874.

Hauenstein, A.J., Zara, J.A., Eversman, W., Qumei, I.K., 1992. Chaotic and nonlinear dynamic response of aerosurfaces with structural nonlinearities. AIAA-92-2547-cp.

Lee, B.H.K., Price, S.J., Wong, Y.S., 1999. Nonlinear aeroelastic analysis of airfoils: bifurcation and chaos. Progress in Aerospace Sciences 35, 205–334.

McIntosh Jr., S.C., Reed Jr., R.E., Rodden, W.P., 1981. Experimental and theoretical study of nonlinear flutter. Journal of Aircraft 18, 1057–1063.

O'Neil, T., Strganac, T.W., 1998. Aeroelastic response of a rigid wing supported by nonlinear springs. Journal of Aircraft 35, 616–622.

Sheta, E.F., Harrand, V.J., Thompson, D.E., Strganac, T.W., 2002. Computational and experimental investigation of limit cycle oscillations of nonlinear aeroelastic systems. Journal of Aircraft 39, 133–141.

Tang, D., Dowell, E.H., 1993. Comparison of theory and experiment for non-linear flutter and stall response of a helicopter blade. Journal of Sound and Vibration 165, 251–276.

Tang, D., Conner, M.D., Dowell, E.H., 1998a. Reduced-order aerodynamic model and its application to a nonlinear aeroelastic system. Journal of Aircraft 35, 332–338.

Tang, D., Dowell, E.H., Virgin, L.N., 1998b. Limit cycle behaviour of a wing section with a control surface. Journal of Fluids and Structures 12, 839–858.

Trickey, S.T., Virgin, L.N., Dowell, E.H., 2002. The stability of limit-cycle oscillations in a nonlinear aeroelastic system. Proceedings of the Royal Society of London 458, 2203–2226.

Woolston, D.S., Runyan, H.L., Byrdsong, T.A., 1955. Some effects of system nonlinearities in the problem of aircraft flutter. NACA TN, 3539.

Yang, Z.C., Zhao, L.C., 1988. Analysis of limit cycle flutter of an wing section in incompressible flow. Journal of Sound and Vibration 123, 1–13.

Zimmerman, N.H., Weissenburger, J.T., 1964. Prediction of flutter onset speed based on flight testing at subcritical speeds. Journal of Aircraft 1, 190–202.